Journal of Coastal Research	17	2	328–341	West Palm Beach, Florida	Spring 2001

Absorption, Scattering, and Remote-Sensing Reflectance Relationships in Coastal Waters: Testing a New Inversion Algorithm

R.W. Gould, Jr.,† R.A. Arnone,† and M. Sydor‡

†Naval Research Laboratory
Remote Sensing Applications Branch
Code 7343
Stennis Space Center, MS 39529, U.S.A.

‡Department of Physics
University of Minnesota Duluth
Duluth, MN 55812, U.S.A.

ABSTRACT

GOULD, R.W., JR.; ARNONE, R.A., and SYDOR, M., 2001. Absorption, Scattering, and Remote-Sensing Reflectance Relationships in Coastal Waters: Testing a New Inversion Algorithm. *Journal of Coastal Research,* 17(2), 328–341. West Palm Beach (Florida), ISSN 0749-0208.

In-water absorption and scattering coefficients, and above-water remote-sensing reflectance are tightly linked and, in coastal waters, exhibit unique spectral characteristics at near-infrared wavelengths. The surface-reflectance is uncoupled from the total, measured reflectance, the corrected remote sensing reflectance is calculated by difference, then the absorption and scattering coefficients are estimated using a new inversion algorithm. The surface correction and inversion algorithms are based on a reflectance difference at 715–735 nm. At these wavelengths, total absorption is due primarily to pure water absorption, and the reflected sky/cloud light and backscattering spectra are nearly flat. Required algorithm parameters, and ultimately the corrected remote sensing reflectance spectra and spectral absorption and scattering estimates, can be refined if *in situ* measurements of absorption at 412 nm and spectral scattering shape are available.

The coupled surface correction/inversion algorithms were tested using data from 14 experiments at five U.S. coastal locations collected over a three-year period and representing a variety of absorption and scattering regimes. The average errors between measured and modeled absorption and scattering coefficients over the 400–700 nm wavelength range were 14.6% and 3.0%, respectively (without regard to sign).

ADDITIONAL INDEX WORDS: *Remote sensing, reflectance, optics, absorption coefficient, scattering coefficient, ocean optics, coastal remote sensing.*

INTRODUCTION

The field of marine optics is directly related to biological oceanography, physical oceanography, and remote sensing, so an understanding of the submarine light field is an essential component of many studies. Apparent optical properties (AOPs), such as remote sensing reflectance (R_{rs}) and the diffuse attenuation coefficient, are dependent on the directional structure of the ambient light field, but they are stable enough to characterize differences between water masses (MOBLEY, 1994). In many cases, spatial and temporal variations in AOPs provide adequate insight into a variety of oceanographic processes, such as qualitative descriptions of river discharge and surface circulation patterns, fish distributions, and sediment transport. Surface reflectance measured synoptically from airborne and satellite sensors provides a unique capability for monitoring these coastal processes.

Inherent optical properties (IOPs), such as the absorption coefficient (a) and scattering coefficient (b), are not dependent on the ambient light field; they are coupled with radiative transfer theory to describe spectral radiance and irradiance distributions in the water. This is known as the "forward" problem in hydrologic optics. The magnitude and spectral quality of the radiance/irradiance fields are in turn required parameters for phytoplankton primary production, biomass, heat flux, and convective mixing models. The "inverse" problem involves estimating IOPs from measurements of the submarine light field and has significance in remote sensing because the submarine light field can be linked to the synoptic surface reflectance measurements. The IOPs can then be used to quantitatively assess regional and temporal differences between water masses.

Reflectance can be measured using in-water instruments (and then extended up though the water surface) or it can be measured above the water surface. However, there are differences between these techniques and problems associated with both. Accurate in-water measurements of the light field and the absorption/scattering coefficients are difficult to achieve for several reasons. For measurements of upwelling radiance (L_u) and downwelling irradiance (E_d), ship and instrument shading must be reduced or accounted for with correction procedures (GORDON and DING, 1992). In turbid, coastal waters, light is attenuated rapidly with depth, and

99108 received 13 December 1999; accepted in revision 8 August 2000.

the attenuation length may be shorter than the length of the instrument, so slight changes in sensor depth severely affect the measurements. Also, it is difficult to measure radiances immediately below the sea surface, so near-surface values are generally extrapolated up to the surface using an average value for the diffuse attenuation coefficient. For comparison with above-water reflectance measurements, the surface radiances must then be extended upward through the air-sea interface, typically by assuming a constant value for the transmission coefficient. Because of these difficulties, an alternative approach is to use above-water reflectance measurements to derive estimates of in-water optical properties.

Above-water reflectance measurements using a hand-held spectroradiometer are not without serious measurement problems as well. These measurements contain both surface-reflectance and water-reflectance components which must be separated (only the water component is related to the water IOPs). The removal of the surface reflectance is problematic and may be a reason why in-water and above-water reflectance measurements differ. The surface reflectance varies spectrally and is dependent on surface waves and foam (*i.e.,* wind), cloud cover, solar altitude, azimuth, and instrument orientation. So, before the inversion problem of deriving water IOPs from above-water reflectance measurements can be solved, the surface reflectance signal must first be removed from the total, measured reflectance values.

Ocean color algorithm development to derive bio-optical properties of the water from radiance or reflectance measurements was initially focused on open-ocean regions, with the impetus provided by large-scale, global remote sensing requirements (GORDON and MOREL, 1983). In the open-ocean, phytoplankton and associated degradation products control the optical character of the water (Case 1 waters—MOREL, 1988). More recently, research efforts have attempted to extend these algorithms (GOULD and ARNONE, 1994), or develop new ones, for the more complex coastal environment (GOULD and ARNONE, 1997; SYDOR *et al.,* 1998; LEE *et al.,* 1998). Because additional factors dominate the spectral signature of Case 2 coastal waters (absorption by dissolved organic matter, scattering by suspended sediments), new algorithms are required that exploit the changes in the magnitude and spectral quality of the submarine light field relative to the open-ocean.

Our objectives are to develop a correction scheme to remove surface-reflected sunglint and sky/cloud light from above-water reflectance measurements and to use these corrected reflectance values in a new inversion algorithm to estimate a and b. To validate the correction and inversion algorithms, model results are compared with *in situ* a and b measurements from a variety of coastal regions.

BACKGROUND

The color of water is related to its inherent optical properties, which are determined by the particulate and dissolved constituents. In the present study, relationships between reflectance, absorption, and backscattering are described (Equations 1–11); a new algorithm to correct for surface reflection is presented (Equations 12–25); and an inversion algorithm is described (Equations 26–33). Optional temperature/salinity and CDOM/detrital adjustments are also discussed (Equations 34–35). We follow standard notation and terminology as described in MOREL and GENTILI (1996), MOBLEY (1999), and TOOLE *et al.* (2000).

Absorption, Scattering, and Reflectance Relationships

Irradiance reflectance R is defined as:

$$R \doteq E_u/E_d, \tag{1}$$

where E_u is the upwelling irradiance and E_d is the downwelling irradiance (both measurements made below the air/water interface; wavelength notation is omitted for brevity unless explicitly denoted). R is related to in-water IOPs (MOREL and PRIEUR, 1977; GORDON *et al.,* 1988):

$$R = fb_b/a, \tag{2}$$

where b_b is the backscattering coefficient and f is an empirical constant equal to about 0.33 (MOREL and PRIEUR, 1977), although it varies with sun angle (MOREL and GENTILI, 1993). Remote-sensing reflectance, R_{rs}, the derived parameter of interest in satellite remote sensing of ocean color, is distinguished from R and is defined as,

$$R_{rs} \doteq L_w/E_d, \tag{3}$$

where L_w is the water-leaving radiance. Here, both L_w and E_d are measured above the air/water interface (from this point, all remaining variables refer to measurements in air unless specified). Unfortunately, it is not possible to directly measure L_w because a radiometer measurement of the sea surface, L_t, contains L_w plus a surface-reflectance component, L_r:

$$L_t = L_w + L_r, \tag{4}$$

where

$$L_r = \rho L_{sky} \tag{5}$$

L_{sky} is the sky radiance (measured). ρ is the sea-surface reflectance factor [commonly set to the Fresnel reflectance but it varies with wind speed and incident angle (AUSTIN, 1972)]. Dividing the radiance terms by E_d to convert to reflectance:

$$R_t = R_{rs} + R_r, \tag{6}$$

where

$$R_r = \rho R_{sky} \tag{7}$$

Measurements and calculations for R_t and R_{sky} are explained in the Methods. R_{rs} is calculated by difference. In the standard SeaWiFS protocol to correct above-water reflectance measurements, R_{rs} at 750 nm is subtracted across the entire R_{rs} spectrum to remove any residual surface reflectance due to wave facets, *i.e.,* sunglint (MUELLER and AUSTIN, 1995; MOBLEY, 1999, TOOLE *et al.,* 2000).

To derive water IOPs from above-water R_{rs} spectra, R_{rs} must be related to R, which differ by a radiance/irradiance conversion factor and by the transfer functions across the air/water interface. Thus:

$$R_{rs}(\lambda) = Cb_b(\lambda)/a(\lambda), \tag{8}$$

where

$$C = [f(1 - r_F)(1 - R_s)]/[Qn^2(1 - RR_u)] \quad (9)$$

The C term combines all the reflection and refraction effects and conversions into one term. See MOBLEY (1999) for a complete derivation. Embedded in C is the Q factor:

$$Q = E_u/L_u, \quad (10)$$

where L_u is the upwelling radiance (here, both E_u and L_u are measured in water). The f/Q ratio varies with nadir viewing angle, azimuth angle, sun zenith angle, wavelength, and bio-optical state and accounts for most of the variability in the C term. The other terms are relatively constant or vary over small ranges (MOBLEY, 1999; MOREL and GENTILI, 1993; 1996). C will also vary with wind speed, which affects air/sea transmission (reflection at the interface). r_F is the Fresnel reflectance of the surface as seen from the water side, R_s is the irradiance reflectance of the surface from the air side, R_u is the irradiance reflectance of the surface from the water side, and n is the seawater index of refraction. In our derivations below, C is assumed spectrally constant for any given reflectance measurement (it can vary from sample to sample, see Discussion), but an explicit estimate of its value is not required, as it is incorporated into a combined term with b_b:

$$C_b(\lambda) = Cb_b(\lambda) \quad (11)$$

This is the numerator of Equation 8. The backscattering coefficient is comprised of water (b_{bw}) and particulate (b_{bp}) components, although the water component is very small at wavelengths from 400–700 nm (SMITH and BAKER, 1981) and can be considered negligible. b_{bp} contains both organic and inorganic particles. The absorption coefficient is commonly separated into water (a_w), phytoplankton (a_ϕ), detrital (a_d), and colored dissolved organic matter (CDOM or gelbstoff, a_g) components (ROESLER *et al.*, 1989), all of which can contribute significantly to total a, depending on wavelength.

A typical R_{rs} spectrum for coastal waters is shown in Figure 1, along with representative curves for the various components that interact to produce the observed R_{rs} signature, according to Equation 8. Note the various curve shapes in the hatched area. The sharp decrease in reflectance at wavelengths over 700 nm is caused by the sharp increase in pure-water absorption. In this near-infrared wavelength region (715–735 nm), there is a strong relationship between the backscattering coefficient and reflectance, because pure-water absorption is the main contributor to total absorption, and the spectral absorption coefficient of pure water is well-defined (POPE and FRY, 1997). Absorption by phytoplankton pigments, detritus, and CDOM are negligible at these wavelengths and the spectral curve shapes are flat (ROESLER and PERRY, 1995; also see Discussion). The spectral shapes of b and b_b are also relatively flat over this narrow wavelength range, with only a 2.8% difference between b(715) and b(735) (using the spectral model of GOULD *et al.*, 1999). These relationships form the basis for our surface correction and inversion algorithms.

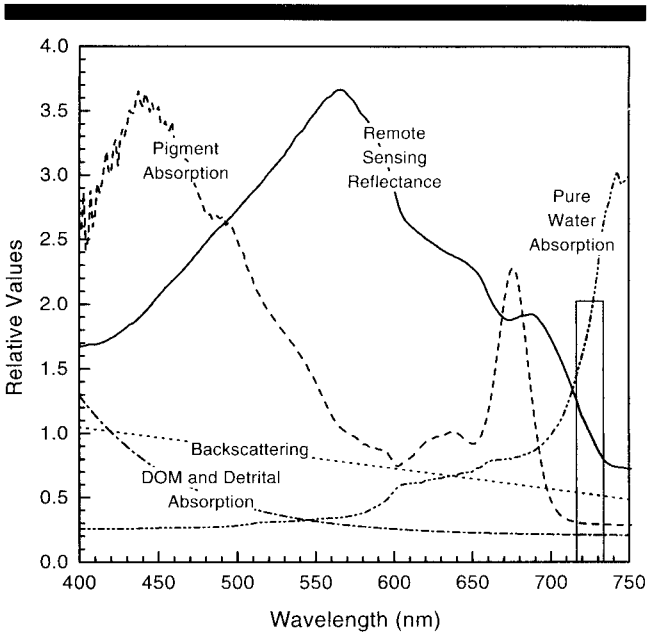

Figure 1. Typical curve shapes for coastal remote-sensing reflectance, phytoplankton pigment absorption, CDOM and detrital absorption, pure water absorption, and backscattering coefficients. The Y axis scaling and units vary for each curve. The curves are overlaid simply to demonstrate how the a and b_b components interact to determine the resulting shape of the reflectance curve, through Equation 8. The 715 to 735 nm wavelength region (hatched area) is used as the basis for our new surface-correction and IOP inversion algorithms. At these wavelengths, the sharp decrease in remote-sensing reflectance is controlled by the sharp increase in pure water absorption (which is well characterized) and by the backscattering coefficient.

ALGORITHM DEVELOPMENT

Before the inversion algorithms can be applied to estimate water IOPs from above-water reflectance measurements, a correction to remove the surface reflection must first be performed, *i.e.*, $R_r(\lambda)$ must be calculated and removed from the measured $R_t(\lambda)$, yielding $R_{rs}(\lambda)$ according to Equation 6. Then, $R_{rs}(\lambda)$ can be incorporated into an inversion algorithm to estimate $a(\lambda)$ and $b(\lambda)$. However, several problems arise with the above relationships to estimate R_{rs}. First, ρ (Equation 5) is only equal to the Fresnel reflectance when the sea surface is flat and the sky radiance is uniform (MOBLEY, 1999). Frequently, this is not the case, making it difficult to estimate ρ. If the sky radiance is non-uniform or if the sea-surface is not flat, the measured L_t values will contain reflected sky/cloud light from outside the L_{sky} measurement cone. This will result in errors of unknown magnitude in the correction for surface reflectance (MOBLEY, 1999; TOOLE *et al.*, 2000). This is a problem for any correction algorithm based on L_{sky} measurements, including minimization and optimization algorithms (LEE *et al.*, 1996; LEE *et al.*, 1997). Also, the standard SeaWiFS protocol applies a bias correction to remove residual reflectance under the assumption that $R_{rs}(750)$ should equal 0. This is not the case in turbid, coastal waters; when the scattering coefficient is high, there is reflectance from particles at red and near-IR wavelengths (SYDOR and ARNONE, 1997). Thus, $R_{rs}(750)$ is not zero and the SeaWiFS protocol removes too much residual reflectance, thereby underestimating the true R_{rs}. A procedure is introduced to correct these

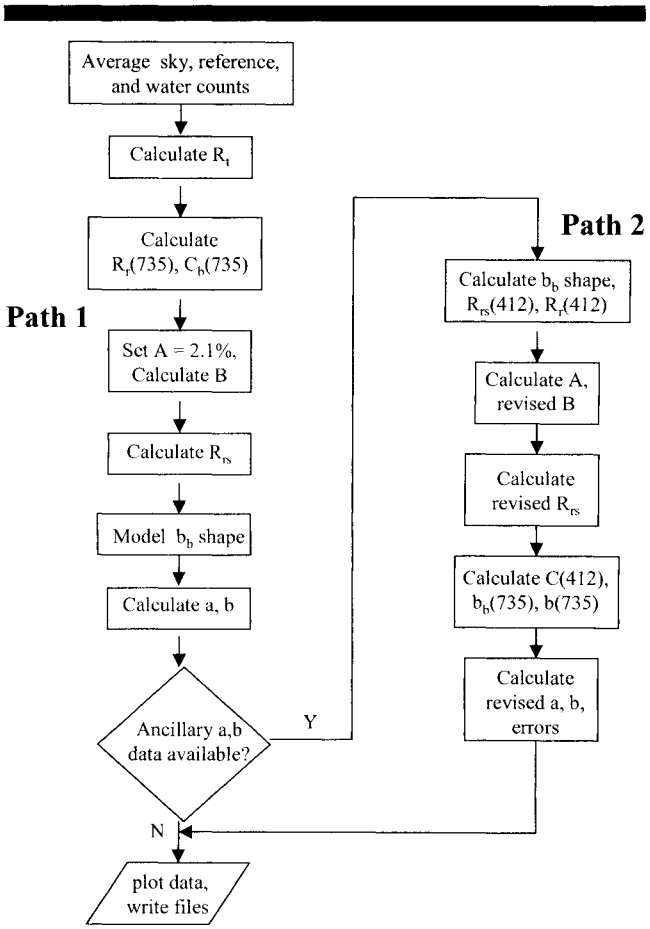

Figure 2. Schematic summary of the processing flow for the surface-correction and IOP inversion algorithms. Two paths are distinguished. Flow diverges and improved parameter estimates are obtained if ancillary measurements of a(412) and b shape are available (Path 2). Parameters are described in the text.

problems by coupling reflectance spectra with *in situ* optical measurements. A ρ value is calculated (our A term, see below) rather than assumed equal to Fresnel reflectance, and a residual offset is calculated (our B term below) rather than assumed equal to $R_{rs}(750)$:

$$R_r = AR_{sky} + B \quad (12)$$

The AR_{sky} term accounts for the spectrally-variable reflected sky light and the B term accounts for the spectrally-flat sunglint and reflected cloud light.

Surface Correction Algorithm

The processing flow of the surface reflectance algorithm and the inversion algorithm is summarized in Figure 2. Two paths are distinguished in the processing flow: for Path 1, no ancillary in-water optical measurements of a(412) and b shape are available. For Path 2, the ancillary data are available to refine algorithm parameters. The surface correction and inversion algorithms are linked; if processing follows Path 2 for the surface correction, it also follows Path 2 for the inversion algorithm. Subscript 1 refers to a wavelength of 715 nm and the subscript 2 refers to 735 nm.

For our surface correction and inversion algorithms, two assumptions are made:

1) spectral R_r is nearly flat over the narrow wavelength range from 715 to 735 nm (see Figure 5):

$$R_{r1} = R_{r2} \quad (13)$$

Thus, from Equation 6:

$$R_{t1} - R_{t2} = R_{rs1} - R_{rs2} \quad (14)$$

2) C is a constant (at any given station) and spectral b_b is nearly flat over that same wavelength range:

$$C_{b1} = C_{b2} \quad (15)$$

From Equation 8:

$$R_{rs1} - R_{rs2} = C_{b1}/a_1 - C_{b2}/a_2 \quad (16)$$

From assumption 2, Equation 16 can be rewritten as,

$$R_{rs1} - R_{rs2} = C_{b2}(1/a_1 - 1/a_2) \quad (17)$$

Substituting R_t for R_{rs}, from assumption 1, and a_w for a (as discussed above, only pure-water absorption contributes to the total absorption coefficient at these wavelengths) and solving for C_{b2}:

$$C_{b2} = (R_{t1} - R_{t2})(a_{w1}a_{w2})/(a_{w2} - a_{w1}) \quad (18)$$

Values of 1.007 and 2.250 m^{-1} are used for a_{w1} and a_{w2}, respectively [NOTE: the POPE and FRY (1997) value for a_{w1} is used and the a_{w2} value is estimated using POPE (1993) and POPE and FRY (1997), because POPE and FRY (1997) present values only up to 727.5 nm and $a_w(735)$ is required]. Inserting Equation 18 into Equation 8 and Equation 8 into Equation 6:

$$R_{t2} - R_{r2} = (R_{t1} - R_{t2})a_{w1}/(a_{w2} - a_{w1}) \quad (19)$$

Solving for R_{r2}:

$$R_{r2} = [(R_{t2}a_{w2}) - (R_{t1}a_{w1})]/(a_{w2} - a_{w1}) \quad (20)$$

At this point processing diverges along Path 1 or Path 2.

Path 1

To perform a spectral correction for R_{rs}, *i.e.*, removal of R_r from R_t, estimates of A and B are required in Equation 12. Taking the estimate of R_{r2} from Equation 20, the measured R_{sky2} value, and setting A equal to a standard value of 2.1% (AUSTIN, 1972), B is calculated by difference using Equation 12. Note that this estimate of B incorporates any error introduced by setting A equal to 0.021 and any error introduced through assumptions 1 and 2. With the estimates of A and B and measurements of $R_{sky}(\lambda)$, $R_r(\lambda)$ is calculated from Equation 12 and finally $R_{rs}(\lambda)$ from Equation 6. This completes the Path 1 processing for the surface correction algorithm. At this point, $R_{rs}(\lambda)$ is incorporated into the Path 1 processing for the inversion algorithm.

Path 2

If ancillary in-water a(412) and b(λ) measurements are available (from an AC9 instrument, for example), additional

parameter refinements are made (Figure 2). First, a least-squares linear regression is applied to the b data:

$$b(\lambda) = G_0 + G_1\lambda \quad (21)$$

where G_0 and G_1 are the regression coefficients (this is a tuning of the generalized equation given GOULD *et al.*, 1999). b and b_b are assumed to have the same spectral shape (see GOULD *et al.*, (1999) for discussion). Normalizing to a reference wavelength, r:

$$b_b(\lambda)/b_b(r) = b(\lambda)/b(r) \quad (22)$$

Thus, $R_{rs}(412)$ is calculated from Equation 8, using the $C_b(735)$ value from Equation 18, Equations 21 and 22, and a reference wavelength of 735 nm:

$$R_{rs}(412) = [C_b(735)b_b(412)]/[a(412)b_b(735)] \quad (23)$$

Then, $R_r(412)$ is calculated as the difference between $R_t(412)$ and $R_{rs}(412)$ according to Equation 6. Estimates for both $R_r(735)$ [from Equation 20] and $R_r(412)$ are now available, as well as measured values for $R_{sky}(735)$ and $R_{sky}(412)$. Thus, the two equations:

$$R_r(735) = AR_{sky}(735) + B \quad (24)$$

$$R_r(412) = AR_{sky}(412) + B \quad (25)$$

are solved simultaneously to calculate A and B, the two unknowns required for the surface correction (Figure 3). Here the A term is calculated, rather than assumed equal to a value of 2.1% as in Path 1. With the revised A and B coefficients spectral R_r is recalculated according to Equation 12 and revised R_{rs} according to Equation 6.

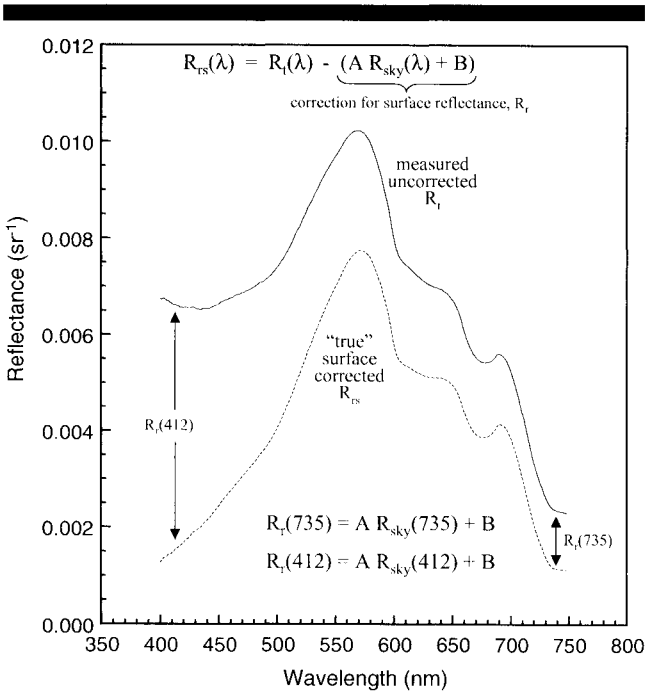

Figure 3. Schematic example of the surface correction for above-water measurements of remote-sensing reflectance. R_t represents uncorrected, above-water reflectance and R_{rs} represents the water reflectance component. The difference between the two spectra represents the surface-reflected sunglint and sky/cloud light, R_r. After calculating R_r at 412 and 735 nm, the two equations are solved simultaneously to estimate the A and B terms. Spectral R_r is calculated by coupling the A and B terms with the measured R_{sky} spectrum. The R_r spectrum is then subtracted from the R_t spectrum to yield the R_{rs} spectrum, which is subsequently used in the IOP inversion algorithm.

Inversion Algorithm

Once the surface reflection has been removed from the above-water R_t measurements, R_{rs} remains, which can be used to estimate spectral a and b. As with the surface-correction algorithm, processing proceeds along two paths depending on whether ancillary optical measurements of a(412) and b(λ) are available to refine parameter estimates. In each case the end products are estimates of spectral a and b, but the calculations and parameter values differ between the two paths.

Path 1

From Equation 8 it is apparent that there should be a strong relationship between b_b and reflectance in the near-IR because total absorption is due mainly to the invariant contribution by the pure-water absorption component. However, we relate the reflectance to b, rather than b_b, because we have measurements of b from an AC9 instrument (see Methods) so we can develop an empirical relationship. b is then related to b_b using the relationship in GOULD *et al.* (1999). Thus, b(555) is estimated from a relationship with ΔR_t (Figure 4):

$$b(555) = 0.30202 + 2.79638\Delta R_t - 0.12928\Delta R_t^2, \quad (26)$$

where

$$\Delta R_t = (R_{t1} - R_{t2})1000 \quad (27)$$

Then, using a spectral scattering model (GOULD *et al.*, 1999):

$$b(\lambda)/b(555) = (1.62517 - 0.00113\lambda)/0.99802 \quad (28)$$

This differs from Equations 21 and 22 that use measured b values to derive the linear regression coefficients that define the spectral shape; here a model is applied. Then b is estimated over the entire wavelength range 400–735 nm by multiplying Equation 28 by the b(555) estimate from Equation 26.

To estimate a, the spectral scattering model of GOULD *et al.* (1999) is used, now referenced to 735 nm, again assuming b_b and b have the same spectral shape:

$$b_b(\lambda)/b_b(735) = (1.62517 - 0.00113\lambda)/0.79462 \quad (29)$$

Then the C_{b2} term ($C{\cdot}b_b$ at 735 nm) from Equation 18, the surface-corrected water reflectance term, R_{rs}, and Equation 29 are coupled to solve for spectral a according to Equation 8:

$$a(\lambda) = [C_{b2}b_b(\lambda)]/[R_{rs}(\lambda)b_b(735)] \quad (30)$$

This completes the processing for Path 1.

Path 2

First, $b_b(412)$ is estimated from the AC9-derived b(412) value following GOULD *et al.* (1999):

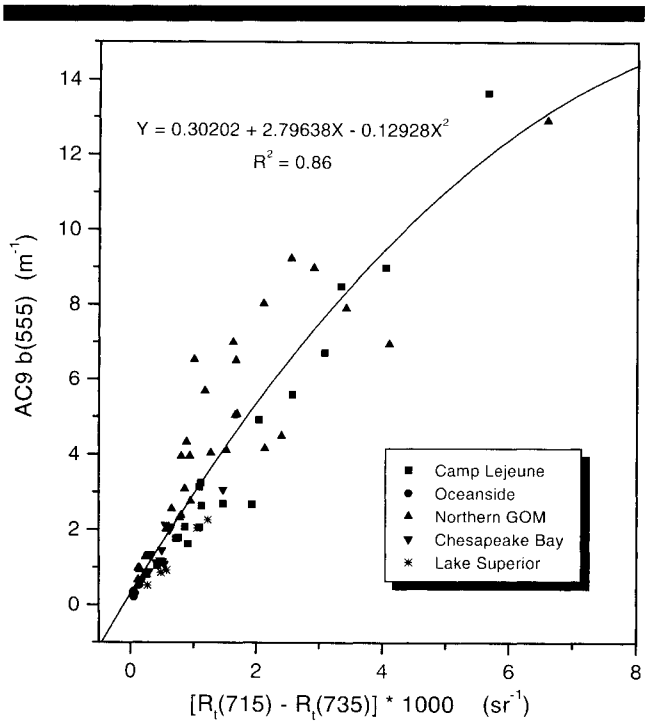

Figure 4. AC9-derived b(555) vs. the reflectance difference $R_t(715) - R_t(735)$. R_t was measured with a field spectroradiometer at the AC9 stations. The solid line represents a least-squares regression fit to the data using a second-order polynomial. Data were collected from five coastal locations over a three-year period.

$$b_b(412) = 0.01829b(412) + 0.00006 \quad (31)$$

Next, the C term at 412 nm is calculated using Equation 8 and $R_{rs}(412)$, a(412), and $b_b(412)$ measurements. Because C is assumed spectrally constant, C(735) is set equal to C(412), then the $C_b(735)$ value from Equation 18 is used to calculate $b_b(735)$ by rearranging Equation 11. b(735) is estimated from $b_b(735)$ (now using the inverse of the b-to-b_b relationship in GOULD *et al.*, 1999):

$$b(735) = 53.56857b_b(735) + 0.00765 \quad (32)$$

Finally, this b(735) value is multiplied by the measured b shape from Equations 21 and 22 (normalized to 735 nm) to estimate b over the 400–735 nm wavelength range:

$$b(\lambda) = b(735)[b(\lambda)/b(735)] \quad (33)$$

Spectral a is estimated as in Path 1 (Equation 30), but the values of the $b_b(\lambda)/b_b(735)$, A, B, R_r, and R_{rs} terms have been adjusted using the Path 2 surface corrections with the *in situ* measurements.

Temperature/Salinity and CDOM/Detrital Adjustments

Two adjustments can be made to the reflectance inversion algorithm: one for temperature and salinity and one for absorption by CDOM and detritus. At near-IR wavelengths, absorption by pure water is strongly affected by temperature, and by salinity to a lesser degree (PEGAU *et al.*, 1997). Thus, if the *in situ* temperature and salinity differ from 22 C and 0 PSU (the values at which the pure-water absorption coefficients were measured), the a_{w1} and a_{w2} values used in Equations 18 and 20 will be in error slightly, as will the calculations of $C_b(735)$ and $R_r(735)$, and subsequently the a and b estimates. If temperature and salinity are measured at a station, the a_{w1} and a_{w2} values can be adjusted following PEGAU *et al.* (1997).

The second adjustment arises from our initial assumption that CDOM and detrital absorption are negligible at near-IR wavelengths. While this is true for most stations, in areas of very high CDOM and/or detrital concentration these components may contribute slightly to the total absorption at 715 nm, even though their spectral shapes decrease exponentially with increasing wavelength (we have observed <10% contribution, even in high CDOM, high scattering river water, with total a(440) values of 7.4 m^{-1}). This small contribution can be accounted for if measurements of a(440) and a(676) are available, from an AC9 instrument, for example.

To account for both detrital and CDOM (gelbstoff) absorption,a combined term (a_{d+g}) is added to each of the pure-water absorption terms in Equation 18:

$$\text{adjusted } C_{b2} = (R_{t1} - R_{t2})(a_{w1} + a_{d+g})(a_{w2} + a_{d+g})/(a_{w2} - a_{w1}) \quad (34)$$

Because the detrital and CDOM spectral absorption curves are flat between 715 and 735 nm, $a_{d+g1} \approx a_{d+g2}$ (so these terms cancel in the denominator) and a_{d+g} is used to represent $a_{d+g}(725)$, the midpoint of the 715 to 735 nm wavelength range. The $a_{d+g}(725)$ term can then be estimated from AC9-measured a(440) and a(676) values and the model of ROESLER *et al.*, (1989). With the adjusted C_{b2}, R_{r2} is calculated from Equations 6, 8, and 11:

$$\text{adjusted } R_{r2} = R_{t2} - [\text{adjusted } C_{b2}/(a_{w2} + a_{d+g})] \quad (35)$$

The adjusted R_{r2} and C_{b2} values are then used throughout the surface correction and inversion calculations, rather than the values from Equations 18 and 20.

The temperature/salinity and CDOM/detrital adjustments have been tested on a few stations from recent experiments (adjusted a values changed by only a few percent). Further evaluation is required before the changes are implemented in our routine processing. The results presented below did not incorporate these adjustments because temperature, salinity, a(440), and a(676) measurements were not available from all stations. Nevertheless, these factors can affect the results and a correction scenario is available.

METHODS

Fourteen surveys were conducted over a three-year period at five locations (off coastal Virginia, California, and North Carolina, in the Northern Gulf of Mexico, and in Lake Superior). Sampling covered all seasons and a variety of environments, including both highly-scattering and highly-absorbing waters (dates and locations are indicated in Table 1). Measurements included spectral R_t, R_{sky}, a, and b. A total of 73 stations are included in the following analyses.

The above-water reflectance measurements are collected with a 512 channel fiber optic Analytical Spectral Devices

Table 1. *Sampling Locations and Dates.*

Location	Number of Experiments	Dates	Number of Stations
Northern Gulf of Mexico	9	7/96, 11/96, 3/97, 7/97, 9/97, 12/97, 4/98, 6/98, 9/98	32
Chesapeake Bay, VA	1	5/97	13
Camp Lejeune, NC	1	4/96	18
Lake Superior	2	7/97 (2)	5
Oceanside, CA	1	10/95	5

(ASD) field spectroradiometer with a 1.4 nm spectral sampling interval over the wavelength range 330–1050 nm. The above-water reflectance method employed uses relative reflectance from a calibrated Spectralon gray card; it does not require a detailed instrument calibration as long as the detector response is linear (MOBLEY, 1999; TOOLE *et al.*, 2000). At each station, five sky, gray card, and water spectra were recorded (L_{sky}, L_g, and L_t, respectively; digital counts, not calibrated radiances) and averaged during post-processing. Measurement integration times were optimized for each target to maximize signal. R_t and R_{sky} values are derived by referencing the averaged water and sky count, respectively, to the averaged counts from the gray card standard of known reflectance (MUELLER and AUSTIN, 1995; MOBLEY, 1999; TOOLE *et al.*, 2000):

$$R_t = L_t/(\pi L_g/R_g) \quad (36)$$

$$R_{sky} = L_{sky}/(\pi L_g/R_g), \quad (37)$$

where R_g is the known gray card reflectance. The spectra were collected at a viewing direction of approximately 30° from nadir and 90° from the sun (LEE *et al.*, 1996). Recent numerical simulations suggest that these angles should be adjusted to 40° and 135°, respectively, to improve estimates of the sea surface reflectance factor (MOBLEY, 1999). The L_{sky} measurements were made in the same plane as the L_t measurements at a 30° zenith angle.

To check the surface-reflectance correction for the above-water R_{rs} measurements, a fiber optic extension cable was attached to the ASD unit and submerged just below the surface of the water on an extension pole, away from any shadowing effects. This provides a direct measurement of the upwelling water radiance, but without the confounding effects of surface reflectance and radiance transfer through the air/sea interface. Thus, the surface-corrected R_{rs} measurements should match the R_{rs} measurements from the submerged probe, if the surface correction is accurate (neglecting air/sea transmission effects). The subsurface measurements were collected from a dock at a test station on the Pearl River in Mississippi. The flat water surface permitted a high degree of control on probe tip submersion depth (~2 cm) and measurement angles (consistent with above-water measurements).

Depth profiles of absorption and beam attenuation (c) at nine wavelengths were collected at each station with a WETLabs AC9 meter. The AC9 instrument is a 25 cm path length, dual-cell instrument. One cell is a cylindrical reflecting tube with a highly polished silvered lining (ZANEVELD *et al.*, 1990). Theoretically, any photons scattered by particles in the enclosed sample will reflect off the chamber walls and into the end detector, so any light attenuation in this chamber should be due to absorption processes only. In practice, however, the detector has a limited acceptance angle, so a scattering correction is required. In addition, the water absorption coefficient in the near-IR is temperature-dependent (PEGAU *et al.*, 1997), so a temperature correction is required as well. Temperature and scattering corrections were applied (following ZANEVELD *et al.*, 1994 and the WETLabs 1998 AC9 User's Guide) and pure-water absorption coefficients (POPE and FRY, 1997) were added to yield total, corrected absorption coefficients.

The other cell of the AC9 instrument has a blackened lining, so any scattered photons will be absorbed by the chamber walls and will not be detected. Thus, light attenuation in this chamber can result from both absorption and scattering processes, so this cell measures total beam attenuation, c, which is the sum of a + b. An estimate of b is derived through subtraction. A rotating filter wheel between the collimated beam illumination source and the sample chambers permits analysis at nine wavelengths (the wavelengths varied slightly between experiments, because more than one instrument was used and the filter sets were not identical). The AC9 surface a and b values were averaged over the upper 1.5m of the water column for comparison with the estimates derived from the R_{rs} inversion algorithm.

RESULTS

Surface Correction

A wide range of R_r spectra were calculated at the coastal stations, due to differences in sun and sky conditions between the sites. The range of magnitudes and shapes for the surface-reflectance correction, R_r, are illustrated in Figure 5, for selected stations. For each R_r spectrum in Figure 5, corresponding sky/cloud conditions, calculated A and B terms, and AC9-measured absorption and scattering coefficients are provided in Table 2. R_r was calculated following Path 2 processing as in Figure 3. The exponential shapes are controlled by the R_{sky} spectra measured at each station (and the calculated A term) and are consistent with other exponential formulations for the surface correction (LEE *et al.*, 1997).

The surface correction routine works well under a wide range of cloud conditions and water types. In Figure 6, uncorrected reflectance spectra are compared with corrected spectra from Path 1 and Path 2 processing and the standard SeaWiFS correction for above-water reflectance measurements (MUELLER and AUSTIN, 1995). For each of the four stations presented in Figure 6, corresponding R_r spectra are plotted in Figure 5 and parameter values are provided in Table 2. The four stations were selected to illustrate several features. In each case, the SeaWiFS correction protocol yielded incorrect R_{rs} spectra in terms of either spectral shape or absolute magnitude.

When the scattering coefficient is small (b(555) less than about 0.5 m^{-1}), all of the measured reflectance at 750 nm is due to surface-reflected sky/cloud light (Figure 6A, Oceanside

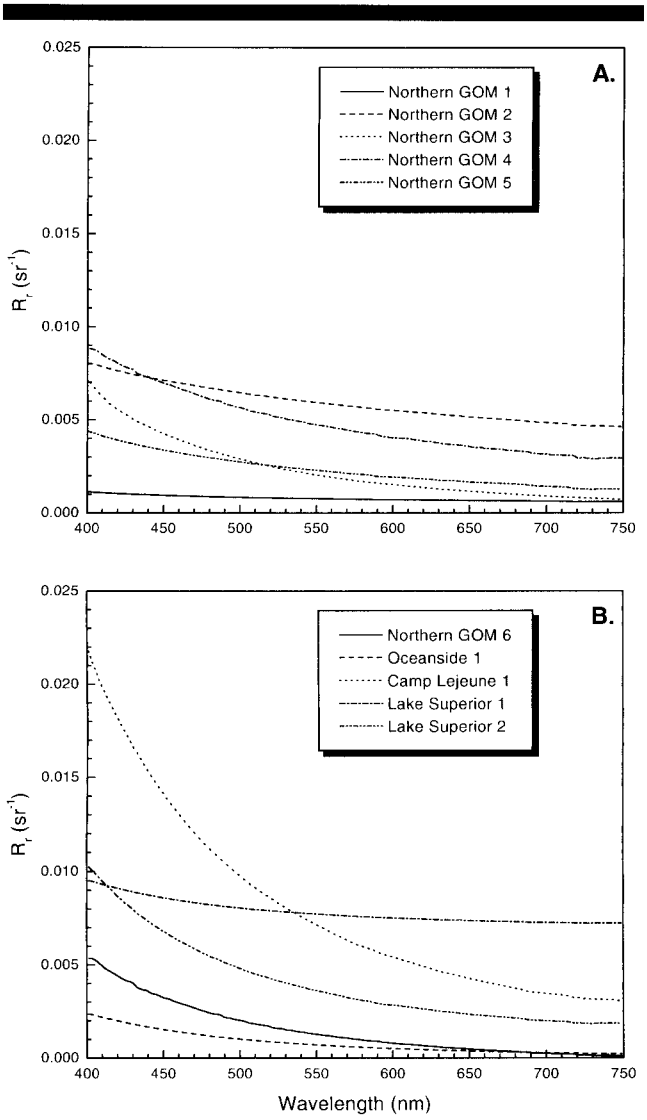

Figure 5. Comparison of R_r spectra calculated for selected coastal stations, to illustrate the range of curve shapes and magnitudes for the surface-reflectance correction. R_r calculated as in Figure 3 (AR_{sky} + B). For each station, corresponding A and B parameter values and AC9-measured absorption and scattering coefficients are presented in Table 2.

Table 2. *Station Characteristics. Selected stations representing a range of sky/cloud conditions, derived A and B values, measured absorption and scattering coefficients.*

Station	Sky/Cloud Conditions	Path 2 A Term	Path 2 B Term (sr^{-1})	ac9 a(412) (m^{-1})	ac9 b(555) (m^{-1})
Northern GOM 1	N/A	0.02019	0.00041	1.76	12.92
Northern GOM 2	70% clouds	0.03273	0.00116	11.58	5.62
Northern GOM 3	clear	0.08152	−0.00006	3.09	6.51
Northern GOM 4	clear	0.07119	0.00050	3.07	7.91
Northern GOM 5	clear w/haze	0.03139	−0.00005	1.00	2.76
Northern GOM 6	N/A	0.07638	−0.00054	1.59	6.99
Oceanside 1	clear	0.05959	−0.00007	0.12	0.36
Camp Lejeune 1	clear	0.16648	0.00060	1.34	6.71
Lake Superior 1	30% clouds	0.04408	0.00691	13.20	15.03
Lake Superior 2	10% clouds	0.16022	0.00079	0.47	0.52

Station 1; Table 2). In other words, in clear Case 1 waters there is no water-leaving radiance at near-IR wavelengths, and at those wavelengths the Path 1 and Path 2 processing corrections agree closely with the bias correction of the standard SeaWiFS protocol (substraction of $R_{rs}(750)$ from all wavelengths). However, only the Path 2 processing yields the correct R_{rs} spectrum at wavelengths from 400–570 nm; R_{rs} spectra from both the Path 1 and SeaWiFS corrections are too high (Figure 6A).

When the scattering coefficient is high, as in turbid Case 2 waters, there is reflectance from particles at red and near-IR wavelengths. Thus, $R_{rs}(750)$ is not zero and the SeaWiFS protocol underestimates the true value (Figures 6B, C, and D). The shape of the R_{rs} spectrum from the Path 1 processing will always match the shape of the spectrum from the SeaWiFS processing because the Path 1 A term is set to 0.021, the same value as in the standard SeaWiFS processing. Only the offset value (B term) is different between the two methods. Figure 6B shows an example where the Path 2-calculated A term (0.166; Camp Lejeune Station 1, Table 2) differs significantly from the Path 1/SeaWiFS value. This results in significant differences between the corrected spectra at blue and green wavelengths. The corresponding R_r spectrum for this station (Figure 5B) exhibits a very sharp increase at blue wavelengths.

In Figure 6C, a station with very high absorption and scattering coefficients and 30% cloud cover (Table 2), the corrected R_{rs} spectra from Path 1 and Path 2 are nearly identical and match the shape from the SeaWiFS processing. However, the 750 nm bias correction of the SeaWiFS processing causes negative R_{rs} estimates at wavelengths <550 nm. This illustrates a problem that was apparent with Coastal Zone Color Scanner (CZCS) imagery and continues to plague SeaWiFS imagery in coastal areas. The SeaWiFS atmospheric correction algorithm incorrectly assumes that all radiance measured at wavelengths 765–865 (channels 7 and 8) is due to atmospheric path radiance. There is, however, signal from the water at these wavelengths in turbid areas. Thus, when the overestimated atmospheric component is extrapolated back to shorter wavelengths and subtracted from the total radiance, the estimates of water-leaving radiances at these shorter wavelengths (412, 443, and 490 nm channels) are often negative (GOULD and ARNONE, 1994; ARNONE *et al.*, 1998; RUDDICK *et al.*, 2000). Of course, subsequent bio-optical algorithms fail in such cases.

Corrected and uncorrected Rrs spectra for a station with approximately 70% cloud cover are shown in Figure 6D (Station Northern GOM 2, Table 2). Path 2 processing yields a large B term due to the large contribution of spectrally flat reflected cloud light across the spectrum. Note the large and relatively flat R_r spectrum for this station in Figure 5A. Path 2 and SeaWiFS-protocol corrections yields similar R_{rs} values at 412 nm, but spectra diverge as wavelength increases.

In Figure 7, above-water, corrected (R_{rs}) and uncorrected (R_t) reflectance spectra are compared with a subsurface spectrum. The spectra were collected from a dock over the Pearl

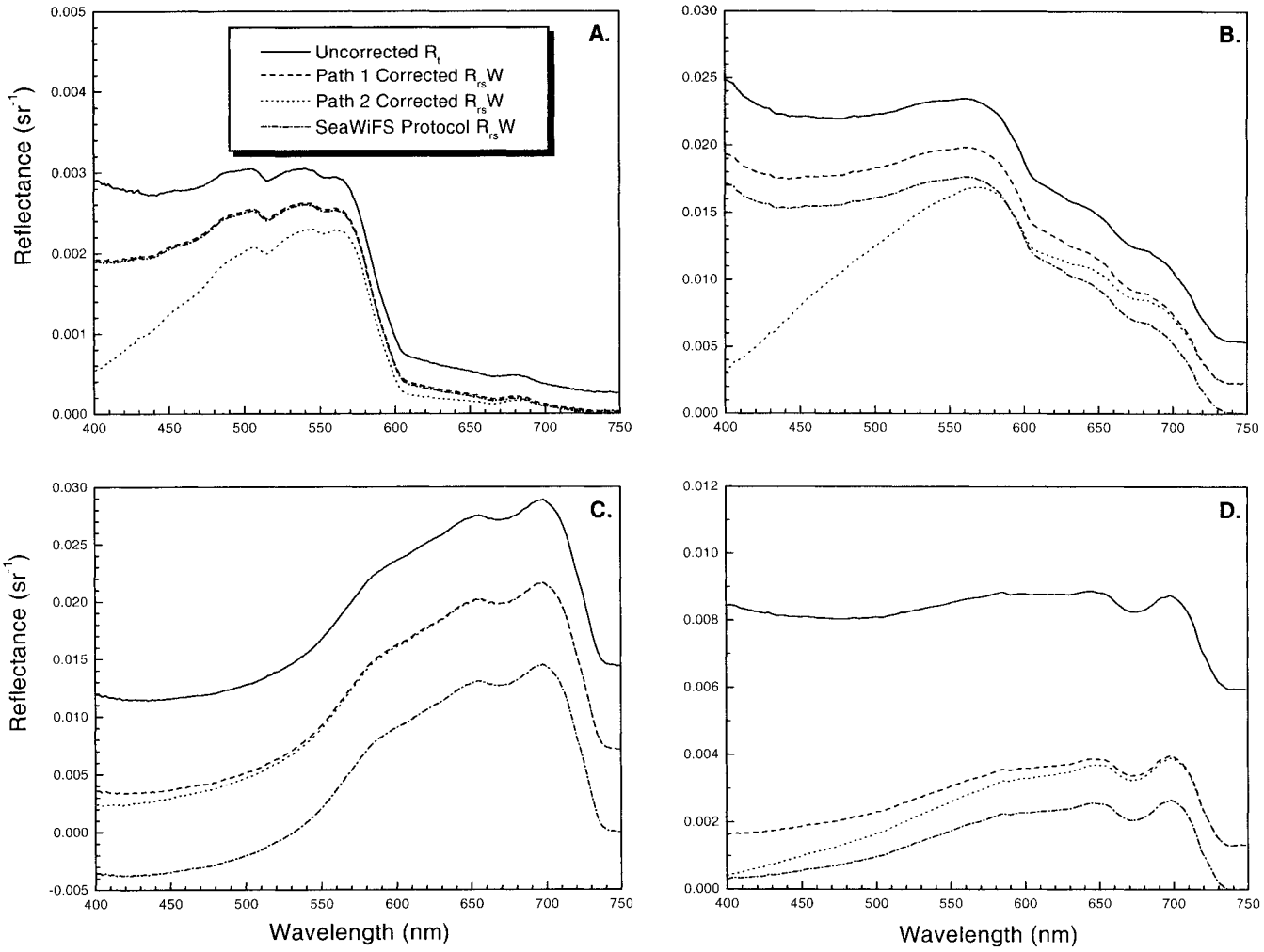

Figure 6. Comparison of uncorrected (R_t) and corrected (R_{rs}) reflectance spectra from four locations. The selected stations represent a range of cloud conditions and absorption/scattering coefficients. Three correction routines are compared: Path 1 and Path 2 corrections as described in the text, and the standard SeaWifs protocol that includes a bias correction (subtracts the residual R_{rs} at 750 nm from all wavelengths). See Table 2 for cloud conditions and coefficient values for each station and Figure 5 for corresponding surface-correction spectra. A. Station Oceanside 1. B. Station Camp Lejeune 1. C. Station Lake Superior 1. D. Station Northern GOM 2.

River in Mississippi (100% clear sky, flat water surface). The subsurface spectrum was collected using fiber optic probe submerged several centimeters below the surface at the same angle as the above-water measurements (30° from nadir, 90° azimuth from the sun). As in Figure 6, results from Path 1 and Path 2 corrections are presented, along with results from the standard SeaWiFs correction protocol. Note the close agreement between the R_{rs} spectrum from the Path 2 correction algorithm and the subsurface spectrum. The measurements collected with the submerged probe do not contain any surface reflection, providing further evidence of the efficacy of our correction algorithm.

Inversion Algorithm

The inversion algorithm was applied to the surface-corrected, shipboard R_{rs} data and the estimated absorption and scattering coefficients were compared with AC9-measured values at the same stations. The reflectance data used in the algorithm were collected with the field spectroradiometer. Both the surface-correction algorithm and the inversion algorithm utilized the ancillary AC9 data to refine required parameter estimates (Path 2 processing). In Figure 8A, the modeled absorption coefficients (lines) are in close agreement with the corresponding measured values (symbols), for six stations from the northern Gulf of Mexico and coastal North Carolina. A similar comparison for the spectral scattering coefficient is shown in Figure 8B. Again, the modeled spectral shapes and magnitudes closely match the measured values.

The percent error between modeled and measured values, for the absorption and scattering coefficients, is calculated as:

$$\% \text{ error} = 100(\text{modeled value} - \text{measured value}) \div \text{measured value} \quad (38)$$

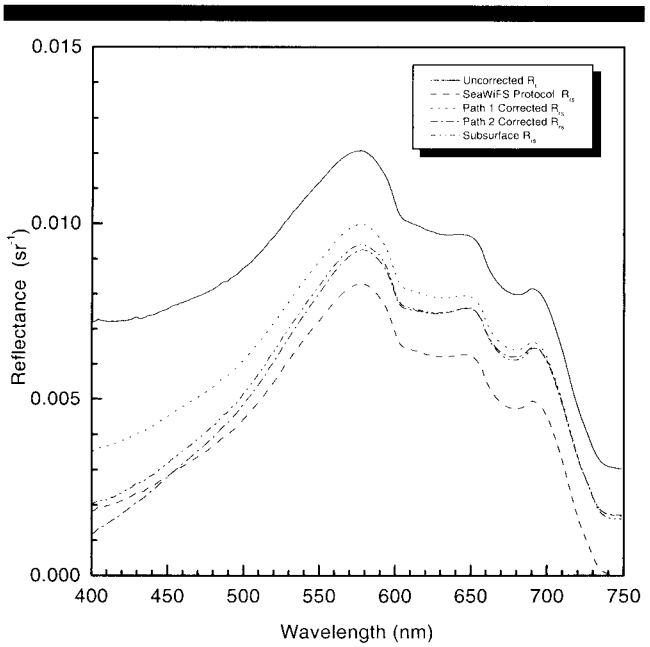

Figure 7. Comparison of uncorrected (R_t), corrected above-water (R_{rs}), and subsurface (R_{rs}) reflectance spectra. Correction routines as in Figure 6. Station from the Pearl River in Mississippi. The subsurface spectrum was collected with a fiber-optic probe attached to the ASD field spectroradiometer and submerged 2 cm below the water surface.

Average error is calculated using the absolute values of the errors, so the average of a 10% error and a −10% error is 10%, not 0.

Following Path 1 corrections, absorption percent errors show systematic variations with wavelength (Figure 9A). Errors are generally negative, indicating modeled values tend to underestimate measured values, and increase with decreasing wavelength from about 550 to 400 nm. This indicates that the assumed value for the A parameter in the Path 1 correction (0.021) is not appropriate; the surface-reflected sky light is not adequately removed from the reflectance spectra before calculating absorption. This error does not affect the spectral scattering estimate (Figure 9B) because that estimate is derived from an empirical relationship based on the reflectance difference in the 715–735 nm wavelength range, a portion of the spectrum that is adequately corrected for surface reflection.

A similar error analysis following Path 2 corrections shows that the systematic spectral bias in the absorption error has been removed (Figure 10A; note that the absorption error at 412 nm is always 0 because the AC9 a(412) value was utilized in the Path 2 surface-reflectance correction, thereby forcing the modeled value to match the measured value). Thus, the removal of surface reflectance from the measured R_t spectra is improved when *in situ* optics measurements are coupled into the correction routine. Relative to Path 1, errors in the scattering coefficient are reduced as well (Figure 10B). Over all wavelengths and locations, for the 73 stations from fourteen experiments, average errors for the absorption and scat-

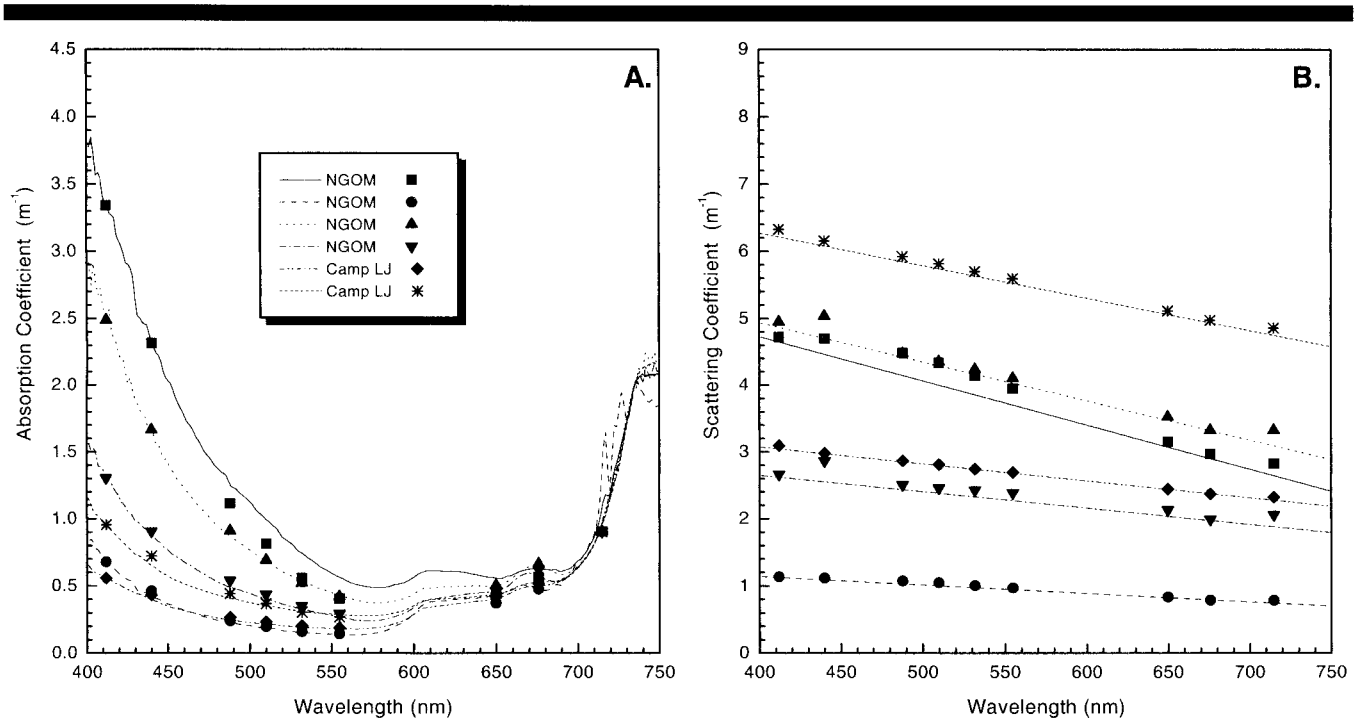

Figure 8. Comparison of measured and modeled spectral absorption and scattering coefficients. Four coastal stations from the northern Gulf of Mexico (NGOM) and two stations off Camp Lejeune, North Carolina (Camp LJ). Lines represent results from our IOP inversion algorithm, following surface correction of the R_t data. Symbols represent corresponding AC9 values. A. Absorption coefficients. B. Scattering coefficients.

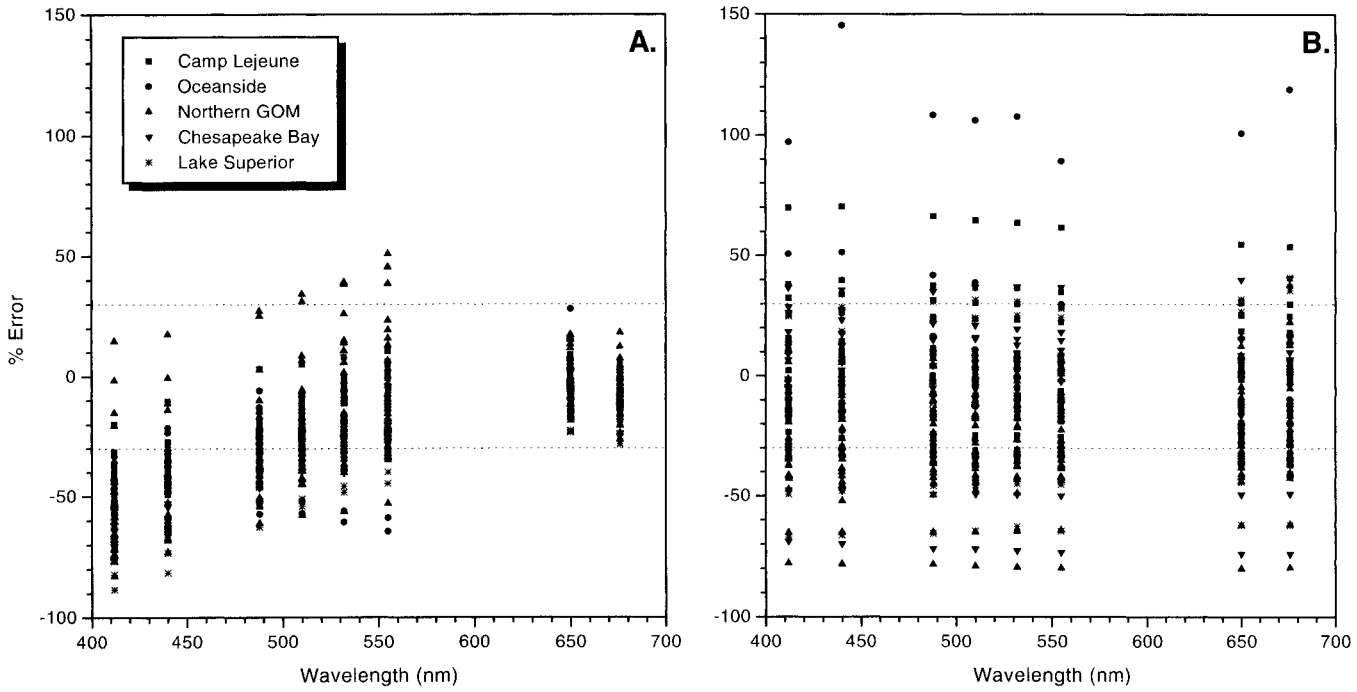

Figure 9. Path 1 error analysis. Measured values vs. modeled results. Errors calculated using Equation 38 after Path 1 R_{rs} correction routine. Average errors over all wavelengths (without regard to sign) are presented in Table 3. Data from 73 stations collected during fourteen experiments at five coastal locations over a three-year period (see Table 1). A. Absorption coefficient. B. Scattering coefficient. Dotted lines indicate ±30% errors, for reference.

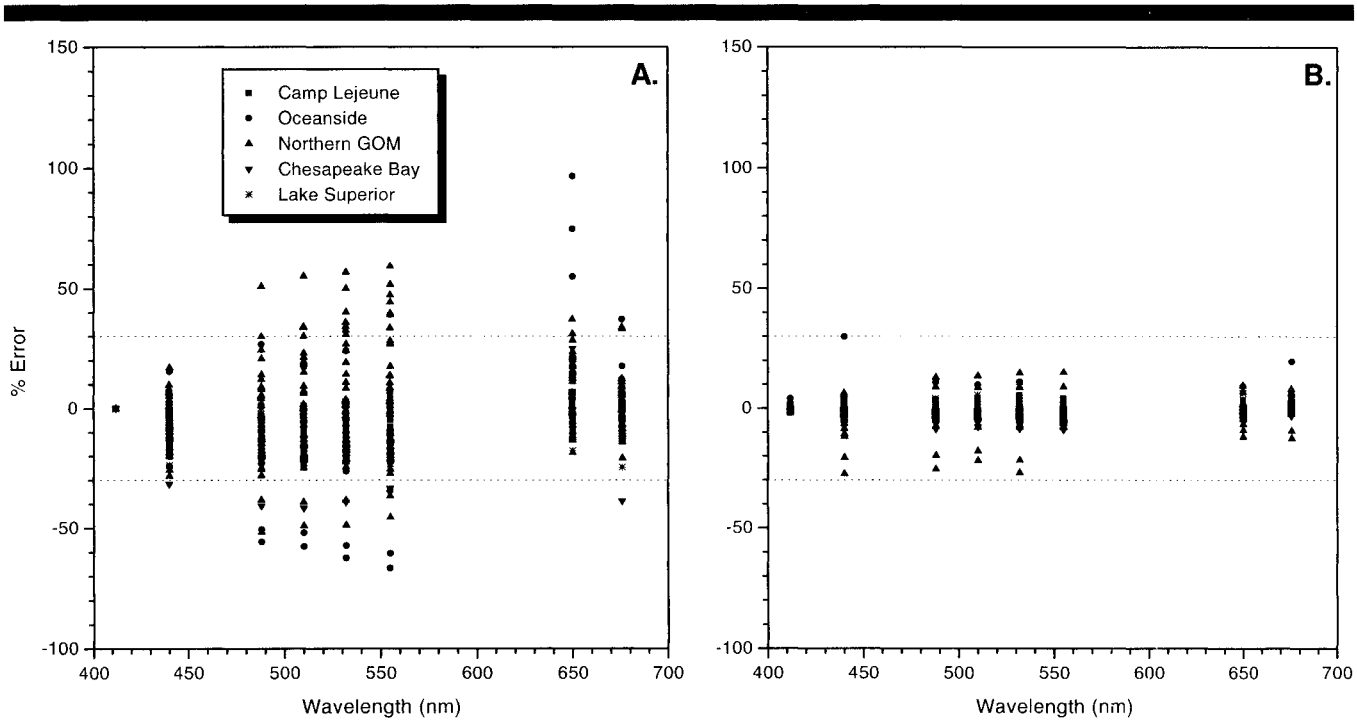

Figure 10. Path 2 error analysis. Measured values vs. modeled results. Data and error calculations as in Figure 9 except after Path 2 R_{rs} correction routine. Average errors over all wavelengths (without regard to sign) are presented in Table 3. A. Absorption coefficient. B. Scattering coefficient.

Table 3. *Parameter and Error Statistics.*

Parameter	Min.	Max.	Mean	Std. Dev.
Path 2 A term	0.02019	0.17938	0.07467	0.03696
Path 1 B term (sr^{-1})	−0.00008	0.00942	0.00116	0.00126
Path 2 B term (sr^{-1})	−0.00155	0.00912	0.00025	0.00125
Path 1 absorption error (%)	0.004	88.35	27.94	19.78
Path 2 absorption error (%)	0.059	96.70	14.61	13.01
Path 1 scattering error (%)	0.006	285.14	28.40	35.48
Path 2 scattering error (%)	0.001	29.85	2.98	3.82

tering coefficients are reduced from 27.9% and 28.4% respectively, following Path 1 processing, to 14.6% and 3.0% following Path 2 processing (Table 3).

DISCUSSION AND CONCLUSION

A new algorithm to correct above-water measurements of R_{rs} for surface reflectance is presented, using R_{rs} measurements at two near-IR wavelengths and coupled *in situ* measurements of a(412) and spectral scattering "shape", if available. A recently-published algorithm to estimate a and b from the surface-corrected R_{rs} values is also modified (SYDOR *et al.,* 1998), and this inversion algorithm is tested using coastal data collected from five sites over a three-year period. The surface correction and inversion algorithms require a reflectance signal in the 715–735 nm wavelength range and therefore are applicable only in turbid, Case 2 waters where suspended sediments reflect strongly at those wavelengths. In clear, open-ocean, Case 1 waters there is very little reflectance signal at near-IR wavelengths. The development, application, and validation of these two algorithms for estimating IOPs in coastal waters is discussed.

The rationale behind the inversion algorithm stems from the wavelength dependence of the various components of absorption and how they contribute to the total absorption coefficient. The algorithm is based on a reflectance difference over a narrow wavelength range in the near-IR region of the spectrum where the reflectance slope is strongly related to the backscattering signal, because the contribution to total absorption from phytoplankton pigments, CDOM and detritus are negligible. Whereas other inversion algorithms require measurements or estimates of the phytoplankton absorption spectrum (ROESLER and PERRY, 1995; LEE *et al.,* 1996; GARVER and SIEGEL, 1997), a highly complex and variable curve, this algorithm only requires a much simpler linear b_b curve shape. As with the surface correction, estimates of a and b are improved if some *in situ* measurements are available to determine the $C_b(735)$ value and the shape of the b_b curve, but a modeled curve shape can also be used.

The effects of inelastic scattering (CDOM and pigment fluorescence, Raman scattering) and bottom reflectance are not considered in the algorithm development. LEE *et al.* (1994) found inelastic scattering to account for <10% of the total remote sensing reflectance in their coastal data set. Also, except for the Oceanside stations, most stations in this study were located in turbid waters with high absorption and scattering coefficients so we expect little contribution from the bottom to the total measured reflectance spectra. However, because the full R_{rs} spectrum is used to derive the $a(\lambda)$ estimates, any bottom reflectance in the R_{rs} spectrum would result in a slight underestimation of a, particularly at wavelengths from about 480–550 nm where bottom reflectance is highest (based on coastal samples from the Gulf of Mexico; LEE *et al.,* 1994).

The bidirectional reflectance structure of the water-leaving radiance affects R_{rs} measurements through the angular dependencies embedded in the C term (Equation 9). Although variations in the magnitude of C between stations are accounted for through our combined C_b term (Equations 11, 18), our assumption that C is spectrally flat is not always true. The spectral variation in the f/Q ratio (MOREL and GENTILI, 1996) will lead to errors in our spectral a estimates from both Path 1 and Path 2 and our spectral b estimate from Path 2. It will not affect the spectral b estimate from Path 1 because that estimate depends only on the reflectance difference $R_t(715) - R_t(735)$ and not on C_b. Incorporation of a "spectral shape" for the C term might further improve the $a(\lambda)$ and $b(\lambda)$ estimates.

Chlorophyll concentration can affect the magnitude and location of the reflectance peak near 700 nm. This affect, however, may be due to several factors, including: chlorophyll fluorescence at 685 nm, anomalous scattering caused by the chlorophyll absorption peak at 675 nm, and/or a combined decrease in phytoplankton absorption coupled with an increase in pure-water absorption (GITELSON, 1992). None of these factors affect our assumption that absorption by phytoplankton pigments is negligible in the wavelength range of interest in our algorithm development (715–735 nm). At these wavelengths, *in vivo* specific absorption coefficients for chlorophyll *b,* chlorophyll *c,* fucoxanthin, and phycoerythrin are 0, and range from only 0.0001–0.0002 m^2/mg for chlorophyll *a* (BIDIGARE *et al.,* 1990). So, even at chlorophyll *a* concentrations of 30 mg/m^3, absorption due to phytoplankton is only 0.006 m^{-1}. High chlorophyll concentration will increase the $R_t(715) - R_t(735)$ reflectance difference (as it should, because this difference is related to the scattering coefficient, and chlorophyll-containing particles are still scatterers), resulting in a larger C_{b2} value (Equation 18) and ultimately higher a and b estimates.

SYDOR *et al.* (1998) presented the basis for the absorption inversion algorithm validated in this paper, but the wavelengths used, the surface-correction algorithm, and the scattering algorithm have been modified. Because this algorithm relies on R_{rs} measurements in the near-infrared region of the spectrum, where water absorption is dependent on tempera-

ture and salinity, optional temperature/salinity and CDOM adjustments have also been added.

Whereas SYDOR *et al.* (1998) used the reflectance difference between 720 and 740 nm, this range is shifted very slightly to use the reflectance difference between 715 and 735 nm, to ensure that reflectance values on the sharply decreasing slope of the R_{rs} curve are used (above 700 nm in Figure 1), and not values on the flat tail. In addition, correlations between b(555) and $R_t(715) - R_t(735)$ were slightly higher than those between b(555) and $R_t(720) - R_t(740)$.

The surface-correction algorithm described here differs significantly from that of SYDOR *et al.* (1998). They use reflectance measurements with and without an attached polarization filter whereas this algorithm relies on R_{sky} measurements coupled with calculated A and B terms. The A and B terms are calculated two different ways, depending on whether *in situ* optical measurements are available. The sea surface reflectance factor (A term) is affected by sky conditions, wind speed, solar zenith angle, and viewing geometry. If it is not estimated accurately, significant errors can occur in the corrected R_{rs} spectra (MOBLEY, 1999; TOOLE *et al.*, 2000). The range of calculated A terms for the stations in this study (0.020–0.179, Table 3) fall within a range of simulated values for a variety of cloud conditions (MOBLEY, 1999; Table 1).

In our Path 2 processing, the above-water R_t measurements are coupled with in-water measurements of a(412), b(412), and scattering shape to correct for surface reflection and improve the resulting R_{rs} spectra. TOOLE *et al.* (2000) present a formulation similar to our Equations 6 and 12 (their Equation 5) with coefficients analogous to our A and B terms. However, they derive coefficient values based on a merging procedure between above-water and in-water reflectance measurements (with in-water measurements extrapolated up to and through the air/sea surface). They present general coefficient values to apply based on two wind states and three cloud conditions whereas we derive unique coefficients at each station. There is agreement that improvements to the standard SeaWiFS correction protocol are required.

For the inversion algorithm, SYDOR *et al.* (1998) calculate the spectral scattering coefficient by assuming a value of 0.051 for the C term in Equation 8, solving for $b_b(730)$, converting to b(730), then using a $1/\lambda$ spectral dependence to estimate $b(\lambda)$. The inversion algorithm presented here does not assume a value for the C term. For Path 1, b(555) is estimated empirically from a reflectance difference then $b(\lambda)$ is estimated using a spectral model. For Path 2, C is calculated from AC9-measured a and b values, $b_b(735)$ is calculated and converted to b(735), then $b(\lambda)$ is estimated from the measured b shape.

Spectral R_{rs} measurements derived from above-water spectroradiometer measurements corrected for sunglint and surface-reflected sky/cloud light with our new method agreed closely with measurements derived from a submerged fiber-optic probe. This technique to remove surface reflectance does not require subsurface or polarized reflectance measurements. However, if measurements of a(412) and the spectral scattering shape are available at the station, algorithm parameter estimates can be refined to improve the surface correction.

Previous work has demonstrated a linear relationship between particle cross-sectional area and the scattering/backscattering coefficients (ROESLER and PERRY, 1995; SYDOR and ARNONE, 1997) and between suspended sediment concentration and reflectance (HAN and RUNDQUIST, 1994; HAN, 1997). At high suspended sediment concentrations, the relationship becomes non-linear (HAN and RUNDQUIST, 1994). We take advantage of these relationships and derive a second-order empirical estimate of b(555) from a reflectance difference in the near-IR. In Figure 4, AC9-derived b(555) values are regressed against $R_t(715) - R_t(735)$. The data were collected from a wide variety of scattering regimes and a single relationship appears valid for the entire data set (although the spread of the data is greater for b(555) values greater than about 5 m^{-1}), suggesting that the scattering/reflectance relationship in the near-IR may have a fairly universal application without geographical limitations or constraints related to differences in particle size and/or composition. In addition, previous work using derivative analysis has shown that the 710–740 nm region of the spectrum correlates well to suspended sediment concentration (CHEN *et al.*, 1992; GOODIN *et al.*, 1993). This is consistent with the approach employed here to estimate the scattering coefficient from the reflectance difference between 715 and 735 nm.

The surface-correction and inversion algorithms were tested using data from fourteen experiments at five U.S. coastal locations collected over a three-year period and representing a variety of absorption and scattering regimes. The mean error between measured and modeled absorption coefficients was 14.6% over the visible spectrum and the mean error for the scattering coefficients was 3.0% (using Path 2 corrections). Future efforts will be aimed at comparing this inversion algorithm with other algorithms and at applying the algorithm to airborne and/or satellite hyperspectral remote-sensing reflectance imagery to derive surface fields of absorption and scattering.

ACKNOWLEDGMENTS

We thank Sherwin Ladner, Greg Terrie, Chris Wood, and Paul Martinolich for assistance with the data collection and processing. Scott Pegau provided the AC9 data set from the Oceanside experiment. This research was funded under the Spectral Signatures of the Coastal Zone (PE61153n), Nesting Satellite Products at Large and Fine Scales (PE62435n), and the Littoral Optical Environment (PE62435n) programs at the Naval Research Laboratory.

LITERATURE CITED

ARNONE, R.A.; MARTINOLICH, P.; GOULD, R.W., JR.; SYDOR, M.; STUMPF, R., and LADNER, S., 1998. Coastal optical properties using SeaWiFS. *In:* ACKLESON, S. and CAMPBELL, J. (eds.), *Ocean Optics XIV,* Proceedings, Hawaii, 10–13 November, 1998 (on CD-ROM, Office of Naval Research, Washington, D.C.).

AUSTIN, R.W., 1972. The remote sensing of spectral radiance from below the ocean surface. *In:* JERLOV, N.G. and STEEMAN NIELSEN, E. (eds.), *Optical Aspects of Oceanography.* New York: Academic, pp. 317–344.

BIDIGARE, R.R.; ONDRUSEK, M.E.; MORROW, J.H., and KIEFER, D.A., 1990. *In vivo* absorption properties of algal pigments. *In:*

SPINRAD, R.W. (ed.), *Ocean Optics X,* Proceedings of SPIE, 1302, 290–302.

CHEN, Z.; CURRAN, P.J., and HANSOM, J.D., 1992. Derivative reflectance spectroscopy to estimate suspended sediment concentration. *Remote Sensing of Environment,* 40, 67–77.

GARVER, S.A. and SIEGEL, D.A., 1997. Inherent optical property inversion of ocean color spectra and its biogeochemical interpretation. 1. Time series from the Sargasso Sea. *Journal of Geophysical Research,* 102(C8), 18607–18625.

GITELSON, A., 1992. The peak near 700 nm on radiance spectra of algae and water: relationships of its magnitude and position with chlorophyll concentration. *International Journal of Remote Sensing,* 13(17), 3367–3373.

GOODIN, D.A.; HAN, L.; FRASIER, R.N.; RUNDQUIST, D.; STEBBINS, W.A., and SCALES, J.F., 1993. Analysis of suspended solids in water using remotely sensed high resolution derivative spectra. *Photogrammetric Engineering and Remote Sensing,* 59(4), 505–510.

GORDON, H.R.; BROWN, O.B.; EVANS, R.H.; BROWN, J.W.; SMITH, R.C.; BAKER, K.S., and CLARK, D.K., 1988. A semianalytic radiance model of ocean color. *Journal of Geophysical Research,* 93(D9), 10909–10924.

GORDON, H.R. and DING, K., 1992. Self-shading of in-water optical instruments. *Limnology and Oceanography,* 37(3), 491–500.

GORDON, H.R. and MOREL, A., 1983. *Remote Assessment of Ocean Color for Interpretation of Satellite Visible Imagery: A review.* New York: Springer-Verlag, 114p.

GOULD, R.W., JR. and ARNONE, R.A., 1994. Extending Coastal Zone Color Scanner estimates of the diffuse attenuation coefficient into Case II waters. *In:* JAFFE, J.S. (ed.), *Ocean Optics XII,* Proceedings of SPIE, 2258, 342–355.

GOULD, R.W., JR. and ARNONE, R.A., 1997. Remote sensing estimates of inherent optical properties in a coastal environment. *Remote Sensing of Environment,* 61, 290–301.

GOULD, R.W., JR.; ARNONE, R.A., and MARTINOLICH, P.M., 1999. Spectral dependence of the scattering coefficient in case 1 and case 2 waters. *Applied Optics,* 38(12), 2377–2383.

HAN, L., 1997. Spectral reflectance with varying suspended sediment concentrations in clear and algae-laden waters. *Photogrammetric Engineering and Remote Sensing,* 63(6), 701–705.

HAN, L. and RUNDQUIST, D., 1994. The response of both surface reflectance and the underwater light field to various levels of suspended sediments: Preliminary results. *Photogrammetric Engineering & Remote Sensing,* 60(12), 1463–1471.

LEE, Z.; CARDER, K.L.; HAWES, S.K.; STEWARD, R.G.; PEACOCK, T.G., and DAVIS, C.O., 1994. Model for the interpretation of hyperspectral remote-sensing reflectance. *Applied Optics,* 33(24), 5721–5732.

LEE, Z.P.; CARDER, K.L.; MOBLEY, C.D.; STEWARD, R.G., and PATCH, J.S., 1998. Hyperspectral remote sensing for shallow waters. I. A semianalytical model. *Applied Optics,* 37(27), 6329–6338.

LEE, Z.P.; CARDER, K.L.; PEACOCK, T.G.; DAVIS, C.O., and MUELLER, J.L., 1996. Method to derive ocean absorption coefficients from remote-sensing reflectance. *Applied Optics,* 35(3), 453–462.

LEE, Z.P.; CARDER, K.L.; STEWARD, R.G.; PEACOCK, T.G.; DAVIS, C.O., and MUELLER, J.L., 1997. Remote-sensing reflectance and inherent optical properties of oceanic waters derived from above-water measurements. *In:* AKLESON, S.G. and FROUIN, R. (eds.), *Ocean Optics XIII,* Proceedings of SPIE, 2963, 160–166.

MOBLEY, C.D., 1999. Estimation of the remote-sensing reflectance from above-surface measurements. *Applied Optics,* 38(36), 7442–7455.

MOBLEY, C.D., 1994. *Light and Water.* San Diego, California: Academic, 592p.

MOREL, A., 1988. Optical modeling of the upper ocean in relation to its biogenous matter content (Case I Waters). *Journal of Geophysical Research,* 93(C9), 10749–10768.

MOREL, A. and GENTILI, B., 1993. Diffuse reflectance of oceanic waters. II. Bidirectional aspects. *Applied Optics,* 32(33), 6864–6879.

MOREL, A. and GENTILI, B., 1996. Diffuse reflectance of oceanic waters. III. Implication of bidirectionality for the remote-sensing problem. *Applied Optics,* 35(24), 4850–4862.

MOREL, A. and PRIEUR, L., 1977. Analysis of variations in ocean color. *Limnology and Oceanography,* 22, 709–722.

MUELLER, J.L. and AUSTIN, R.W., 1995. Volume 25, Ocean Optics Protocols for SeaWiFS Validation, Revision 1. *SeaWiFS Technical Report Series. In:* HOOKER, S.B.; FIRESTONE, E.R., and ACKER, J.G. (Eds.), NASA Technical Memorandum 104566, NASA Goddard Space Flight Center, Greenbelt, Maryland, 67p.

PEGAU, W.S.; GRAY, D., and ZANEVELD, J.R.V., 1997. Absorption and attenuation of visible and near-infrared light in water: dependence on temperature and salinity. *Applied Optics,* 36(24), 6035–6046.

POPE, R.M., 1993. Optical absorption of pure water and sea water using the integrating cavity absorption meter. Ph.D. Thesis, Texas A&M University, College Station, Texas.

POPE, R.M. and FRY, E.S., 1997. Absorption spectrum (380–700 nm) of pure water. II. Integrating cavity measurements. *Applied Optics,* 36(33), 8710–8723.

ROESLER, C.S. and PERRY, M.J., 1995. *In situ* phytoplankton absorption, fluorescence emission, and particulate backscattering spectra determined from reflectance. *Journal of Geophysical Research,* 100(C7), 13279–13294.

ROESLER, C.S.; PERRY, M.J., and CARDER, K.L., 1989. Modeling *in situ* phytoplankton absorption from total absorption spectra in productive inland marine waters. *Limnology and Oceanography,* 34(8), 1510–1523.

RUDDICK, K.G.; OVIDIO, F., and RIJKEBOER, M., 2000. Atmospheric correction of SeaWiFS imagery for turbid coastal and inland waters. *Applied Optics,* 39(6), 897–912.

SMITH, R.C. and BAKER, K.S., 1981. Optical properties of the clearest natural waters. *Applied Optics,* 20(2), 177–184.

SYDOR, M. and ARNONE, R.A., 1997. Effect of suspended particulate and dissolved organic matter on remote sensing of coastal and riverine waters. *Applied Optics,* 36(27), 6905–6912.

SYDOR, M.; ARNONE, R.A.; GOULD, R.W., JR.; TERRIE, G.E.; LADNER, S.D., and WOOD, C.G., 1998. A new remote sensing technique for determination of the volume absorption coefficient of turbid water. *Applied Optics,* 37(21), 4944–4950.

TOOLE, D.A.; SIEGEL, D.A.; MENZIES, D.W.; NEUMANN, M.J., and SMITH, R.C., 2000. Remote-sensing reflectance determinations in the coastal environment: impact of instrumental characteristics and environmental variability. *Applied Optics,* 39(3), 456–469.

WETLABS, INC., 1998. *AC9 User's Guide.* Philomath, Oregon, 34p.

ZANEVELD, J.R.V.; BARTZ, R., and KITCHEN, J.C., 1990. A reflective-tube absorption meter. *In:* SPINRAD, R.W. (ed.), *Ocean Optics X,* Proceedings of SPIE, 1302, 124–136.

ZANEVELD, J.R.V.; KITCHEN, J.C., and MOORE, C., 1994. The scattering error correction of reflecting-tube absorption meters. *In:* JAFFE, J.S. (ed.), *Ocean Optics XII,* Proceedings of SPIE, 2258, 44–55.